HIGH-RESOLUTION SPECTROSCOPIC OBSERVATIONS OF HERBIG STARS V1295 AQL. II.

H. N. Adigozelzade [a]*, ***N. Z. Ismailov*** [a], ***U. Z. U.Z.Bashirova*** [a]

[a] *Tusi Shamakhy Astrophysical Observatory of the Science and Education Ministry of AR Settl.Y.Mammadaliyev, Shamakhy, Azerbaijan, AZ5626*

In this work we continue the spectral study of the unusual Ae Herbig star HD 190073 with pole-on orientation of the rotation axis. In the second part of spectral studies of the HD190073, we examined long-term spectral variations for 2016-2023. Using synthetic spectra of standard stars, extracted profiles of the circumstellar structure for the hydrogen and H and K CaII lines were obtained. All of these lines are show a P Cyg profile in which the deep absorption on the blue wing is highly variable. Long-term variability of spectrophotometric parameters is detected for the lines of hydrogen, helium and other elements. On the character of the long-term variability over time, there is a general cycle of about 38-12 years. A stellar companion or massive planets may cause the reasons for such variations.

Analysis of the Fourier spectrum showed a complex nature of variability. Some periods found in the spectrum and brightness are close and determined with high reliability. From short periods $P_2 = 4 \pm 0.5$ days, and from relatively long periods $P_3 = 97 \pm 3$ days are reliably established. The fundamental parameters and evolutionary status of the star have been determined.

Keywords: Pre-Main Sequence stars – circumstellar disks – disk accretion – individual: HD 190073

1. INTRODUCTION

For the Pre-Main Sequence (PMS) stars with low (T Tauri Stars, TTS) and intermediate mass (Herbig Ae/Be stars, HAeBes) magnetic fields play an important role in the course of evolution. Magnetic fields can be involved in the transfer of angular momentum from the disks themselves at very early stages of starformation, which can change the initial conditions of the star evolution. It is assumed

)https://doi.org/10.59849/2078-4163.2024.2.56

* E-mail: hadigozalzade@gmail.com

that accretion from the disk onto the stellar surface occurs along magnetic field lines [12, 18, 25].

The interaction of the star with its surrounding disk in classical T Tauri stars (CTTS) is well described by the magnetospheric accretion (MA) models [5]. However, it is unclear how well this model can be applied to HAeBes , whose magnetic fields are about an order weaker [3, 13, 14].

To diagnose the magnetosphere in HAeBes type stars, a method is often used that is based on searching for the cyclic variability of the parameters of spectral lines formed in the near region of interaction of the accretion disk with the star. A review of such methods is given, in particular, in the work of [28]. In this work we continue the spectral study of the unusual Ae Herbig star HD 190073 with the orientation of the rotation axis relative to the observer close to the pole $vsini = 3.19 \pm 2.45$ km/s, $i = 34 \pm 2°$, [1]. It is from this angle that one can observe the circumstellar envelope, where the gas has the least studied structure and kinematics. This is the boundary region between the wind zone and the accretion flow falling on the star at high latitudes [19–27].

Our first article [4] was devoted to the search for rapid spectral variations in a star based on homogeneous spectral material obtained at the 2 m telescope of the Shamakhy Astrophysical Observatory of Azerbaijan Ministry of Science and Education for 2015-2023 [4]. In this paper, we present the results of observations for 2016-2023, based on materials obtained with a resolution 28000. Detailed information about the observational spectral material is given in the first part of our work.

2. FEATURES OF THE H AND K CAII LINES

First of all, we note that the profiles of the H and K CaII lines in the spectrum of the star HD 190073 have always aroused great interest due to their unusual structure. Thus, [23] drew attention to the complex absorption structure of the lines of this doublet. In the work [27] presented in detail the results of studies of the unusual structure of these lines. Both doublet lines have several strong absorption components, which are variable, but quite stably maintain their position both in intensity and wavelength over a period of tens of years.

[27] showed that the multicomponent absorption structure is variable with characteristic times ranging from a month to ten years. [29] showed that the radial velocities of the faster component are related to the velocities of the second component in a 2 : 1 ratio. He proposed a pure scattering model to explain the emission of CaII ions from the stellar atmosphere, following a scenario developed by [37]. However, [33] concluded that such ratios do not appear to be sufficient. Only part of the characteristics correspond to the ratio, and these absorptions are

not the strongest among other blue-shifted components of the profile. [33] analyzed 24 samples of the spectrum of HD 190073 obtained from 1943 to 1974 and found a correlation between the structure of the H, K CaII profiles and P Cyg absorptions in Balmer line profiles.They found that the fusion between the two components CaII at -180 and -300 km/s tended to appear and the first of them became stronger than the second when the Balmer line absorption components were deep and broad in the blue-shifted profiles . They explained these correlations within a model based on the selective effects of radiated energy [34, 35].

Figure 1 shows averaged over all dates the H and K CaII line profiles obtained in our observations in 2016-2023. The individual components of the doublet are designated by the symbols H1, H2, H3 and K1, K2, K3, respectively. Solid lines show average profiles, dotted lines show standard deviation from the average intensity. As can be seen from Fig.1, each doublet line has 3 relatively stable absorption components. For the first component, both H1 and K1 have peak shifts of -0.5 ± 2 km/s, i.e. close to the velocities of the star's mass center. The remaining two components H2, H3 and K2, K3 have approximately the same displacement, equal to -180 and -300 km/s, respectively, with a standard deviation from the average ± 6 km/s. The same H and K line profiles of CaII were previously observed by [36] and [32].

As can be seen from Fig.1 as a whole, the observed three absorption components of the doublet have the same displacements, which are consistent with the data of the above-mentioned works. The standard deviation from the average intensity shows that the strongest change in intensity is observed in the component (K3, H3) which has a displacement of about -300 km/s. In addition, the structure of the standard deviation line (dotted line) forms two peaks with an attenuation in the center corresponding to each absorption peak. This is especially clearly visible from the K line profile CaII. In addition to photospheric absorption lines, doublet lines H, K CaII also contain significant emission, which can be formed in the circumstellar disk or in the chromosphere of the star. This line profile of the H, K CaII doublet differs significantly from the line profiles of hydrogen, helium and other elements, which significantly complicates the understanding of their origin, and, as noted above, is one of the controversial issues. To correctly interpret the structure of these lines, it is important to separate the contribution of the radiation from the purely emission component. To clear the contribution of the stellar photosphere in these lines, it is necessary to subtract the line profile of the standard star from the observed line profile. To do this, you need to correctly establish a model of the synthetic spectrum, which is more suitable for the spectrum of the star HD 190073. Since weak lines of metals can often contain additional line or continuous emission, such lines are not suitable for selecting a synthetic spectrum. For this we decided to use the wide wings of the Balmer

series hydrogen lines.

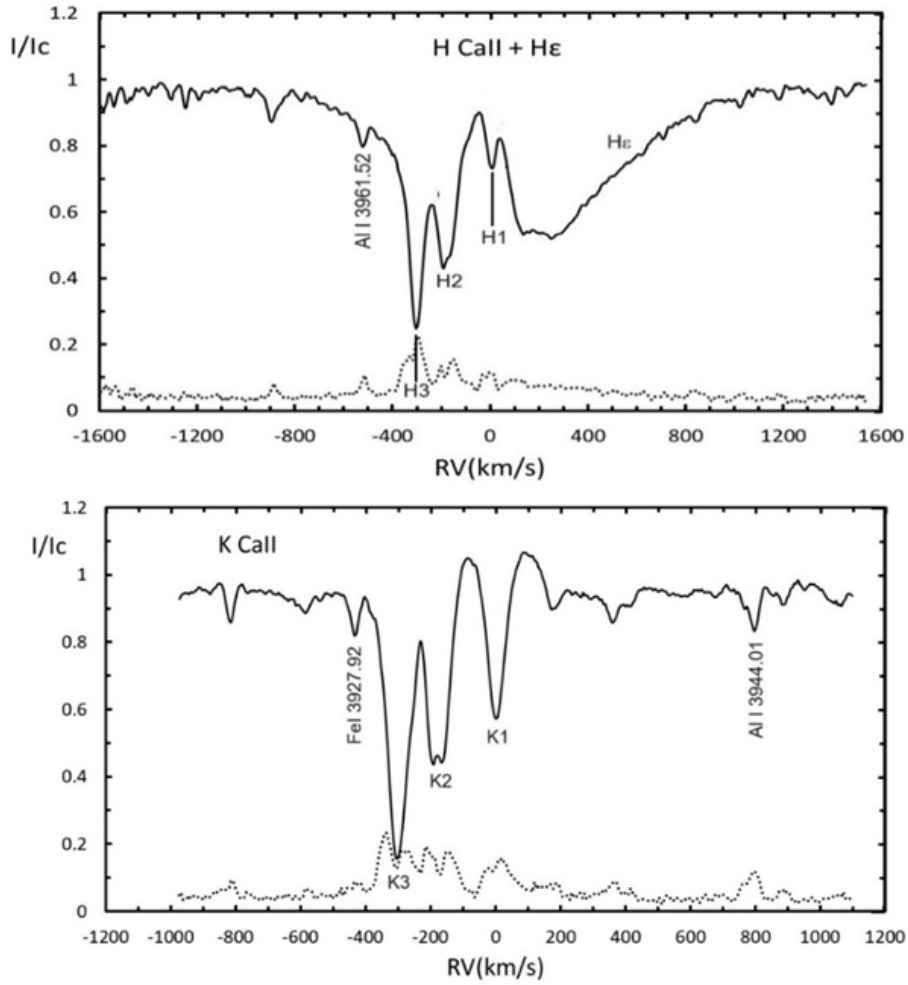

Fig. 1. Average H and K line profiles CaII obtained in 2016-2023. Solid lines show H line profiles CaII $+H_\varepsilon$ (top), and K CaII (bottom). The dotted lines show the level of standard deviation from the average intensity. The individual components of the doublet are designated, respectively, H1, H2, H3 and K1, K2, K3.

3. HYDROGEN LINE PROFILES

Since many photospheric lines in a star's spectrum contain emission components, comparing synthetic and observed spectra based on metal lines can lead to erroneous results. Therefore, to clarify which synthetic model of the spectrum

corresponds to the observed spectrum of the star, we used hydrogen line profiles. Despite the fact that the hydrogen lines of the Balmer series also contain emission in the center, the photospheric Stark wings of these lines are very wide and for the Hβ, Hψ and Hδ lines they are practically not distorted by emission. Therefore, we combined the wings of the hydrogen lines with model profiles in the synthetic spectrum. To select the model, we used the database of synthetic spectra from the PHδENIX archive. Since the literature gives different values for the temperature and gravitational acceleration of a star (see, for example, $8750 \sim K, \log g = 3.0$, [8], $9250 \sim K, \lg g = 3.5$ [2,7] $9750 \sim K, \lg g = 3.5$ [40], we checked all possible values of temperature and gravity acceleration. Synthetic spectra were selected in the range of effective temperatures $8750, 9000, 9250$ and 9500 , at $\log g = 3.0, 3.5, 4.0$ and with chemical composition $[\mathrm{Fe/H}], 0.0, 0.5, 1.0$. Since radial velocities along photospheric lines are close to zero, and the rotation velocity is ~ 3.2 km/s [1], no additional corrections were applied to the broad hydrogen line profiles in the synthetic spectra. After some tests, it became clear that for our spectral resolution, when combining the wings of the Hβ, Hγ and Hδ lines, it is practically impossible to distinguish between models of synthetic spectra with effective temperatures of $9250, 9000$ K and 8750 K at $lgg = 3.0$. We chose the most suitable model with parameters $T_{\mathrm{eff}} = 9000 \pm 250$ K, $\log g = 3.0 \pm 0.1$, $[\mathrm{Fe/H}] = 1.0$. These parameters correspond to the A2III spectral type [31], and are in satisfactory agreement with the data of [8]. After the best alignment of the wings of the hydrogen lines, we subtracted the synthetic normalized profiles from the observed ones. The extracted spectrum profile represents an emission spectrum of nonphotospheric origin.

Figure 2 shows the average profiles for individual Hα-Hδ lines. In Fig. 2, the solid line is the observed normalized profile, the small broken line is the synthetic normalized profile, the broken line indicates the star-model difference profile, and the dotted line shows the standard deviation from the average for the difference profile. One of the intensive emission lines of FeII 4351 observed on the red wing of the Hγ line, which apparently significantly distorts the true intensity level of the red wing of the Hδ line. The best agreement was obtained for the Hβ and Hδ lines. As can be seen from Fig. 2, all dotted lines indicating the standard deviation from the average have two peaks, which are symmetrically located relative to the center of the line. These peaks indicate at what wavelength the intensities change the most. Consequently, we observe the greatest change in the blue and red wings of the lines. This means that, apparently, the variability of the line intensity changes due to the ejection and fall of matter on the surface of the star.

As can be seen from Fig. 2, all difference profiles, without exception, have a single emission peak, for which the ratio of residual intensities $H_\alpha : H_\beta : H_\gamma : H_\delta$ is equal to 6.17:1.04:0.65:0.42.

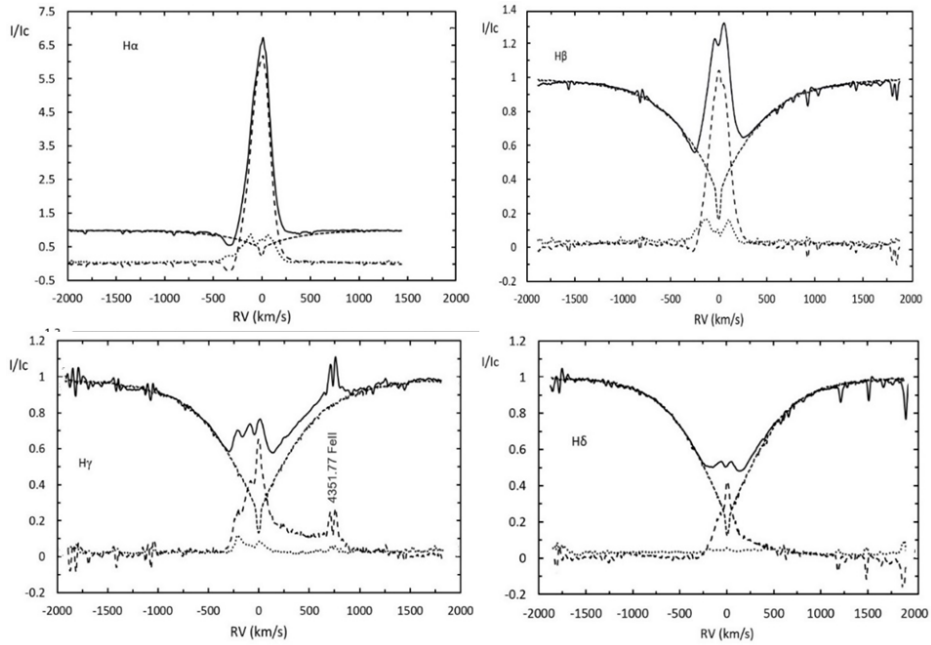

Fig. 2. Hα- Hδ line profiles. Solid line, normalized observed profile, small dotted line, synthetic normalized profile, large dotted line, star - model extracted difference profile ($T_{eff} = 9000K$, log g =3.0, [Fe/H]=1.0), dotted line - standard deviation of intensity along the extracted profile.

4. EXTRACTED PROFILES OF H, K CAII LINES

On the obtained parameters of the star's photosphere, we constructed a difference (extracted) spectrum also for the profiles of the H and K CaII lines. Figure 3 shows the profiles of these lines in two different panels. The figured line designations are the same as in Fig.2. As can be seen, the extracted profile consists mainly of three components. In fig.3, the extracted profile of the K CaII line shows the velocities of individual details. One of them, the purely emission component, is more intense and symmetrical relative to the velocity of the star's center of mass and is divided into two peaks. The displacements of these emission peaks are -58 and +63 km/s, respectively. The second component has two absorption detail with displacements of -196 and -161 km/s. Finally, the third absorption component is shifted by approximately -300 km/s. This component also observed in the ordinary observational profile. We believe that it is formed in a strong accretion zone from the disk. Similar components are observed also in the H CaII line.

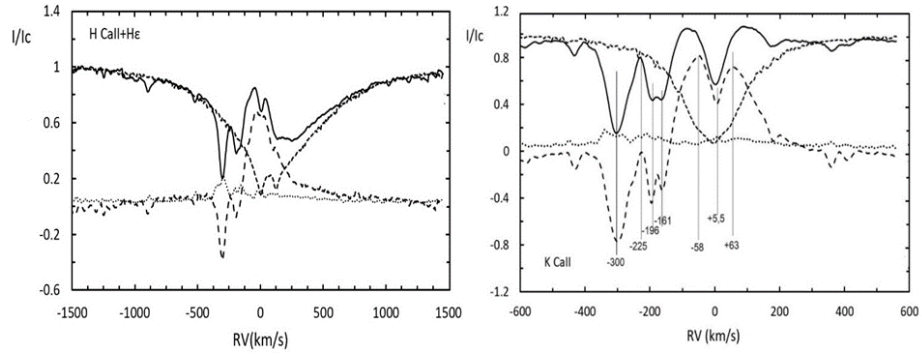

Fig. 3. H and K line profiles of CaII. Designations are the same as in Fig. 2. The second panel shows the radial velocities of individual features in km/s.

5. LONG TIME SPECTRAL VARIABILITY

In the Figure 4 shown the time variability of individual spectrophotometric parameters of the Hα and Hβ lines. The upper panels, from left to right, shows the equivalent widths of the emission components EW_e of the Hα and Hβ lines. The lower panels show the bisector radial velocities of the RV_{bis} emission components, as well as the FWHM of these lines. As can be seen from Fig. 4, from 2015 to 2023, all parameters shows a slow and smooth variability from year to year. The presented cycle covers 9 years of observation, and apparently the full cycle of slow variations should be at 38 years. At the same time, the spread of data over individual years indicates the existence of rapid variability, from several days to months.

As can be seen from Fig.4, the total range of variations in the radial velocities of the emission components for both lines is about 50 km/s. When the lines shift to the red part, a decrease in the total of the FWHM lines is observed, and the equivalent widths gradually decreased. This is especially clearly seen from the $H\beta$ line data. The average value of the FWHM parameter for the Hα line is 4.6 ± 0.3 Å, and for the Hβ line, it is about 2.99 ± 0.5 Å, which corresponds to an expansion of 210 ± 13 km/s and 186 ± 20 km/s, respectively. At 10% of the total residual intensity, the Hα and $H\beta$ line widths reach 9 ± 1 Å and 7 ± 1 Å, which is approximately twice larger, -420 and 370 km/s.

Figure 5 shows the temporal variability in the parameters EW$_e$, RV_{bis} and FWHM for the HeI 5876 line. As can be seen, there is variability that is similar to that observed in the hydrogen lines. As shown in our paper I, hydrogen lines have P Cyg type profiles, where the emission peaks on the blue and red wings have absorption. Let us recall that we denoted the absorption equivalent width on the blue wing of the emission component as EW_{a1}, on the red wing as EW_{a2}, and

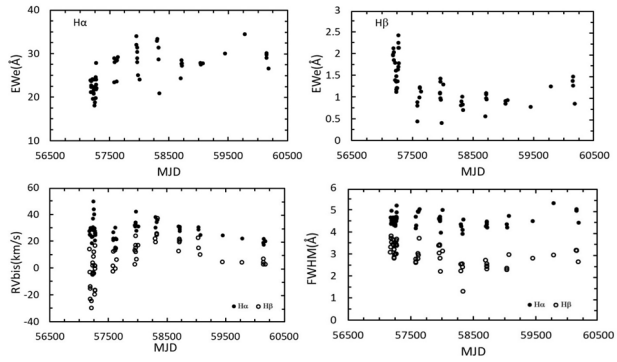

Fig. 4. Time variability in the spectrophotometric parameters of the Hα and Hβ lines.

the equivalent width of the emission component as EW_e . As was shown in article I, with an increase in the intensity of the absorption component on the blue wing of the emission, a synchronous variation in the spectrophotometric parameters of the hydrogen lines was observed.

Figure 6 shows the dependence of some parameters on the equivalent width of the blue absorption component EW_{a1} for the Hβ line. As can be seen, the EW_{a2} and RV_{bis} parameters have a direct correlation, and the EW_2 and FWHM parameters have an inverse correlation with the equivalent width of the blue component EW_{a1}. The value of the Spearman correlation coefficient and its error of determination are shown in each panel of the figures. For the Hα line, the correlation between similar parameters is close to zero. This indicates that the Hα line is formed under more complex conditions.

The observed relationships can be explained as follows. When EWa1 increases, it is because the emission, often seen as a separate weak component of the main emission peak, is red-shifted and appears to enhance the emission in the main emission. This should lead to a decrease at the half-width of the emission line, which could create a visible red shift in radial velocity. This all means that we often see a release, or outflow of matter, which is observed in the form of a weak emission. At the very beginning of its appearance, this peak has a high negative RV, about 450 km/s. Then gradually its RV drops down to a small redshift, which is observed at the main constant emission. Figure 7 shows emission profiles cleared from the photospheric spectrum for different dates in the Hα and Hβ lines. As can be seen, the emerging emission peak on the blue wing of the Hα line gradually merges with the main, more stable red emission peak. Hα line profiles obtained sequentially on close dates show a gradual merging of the blue emission peak with the red one over approximately 20 days, and on July 17, 2017, we already observe a single enhanced emission peak. Hα line profiles do not show

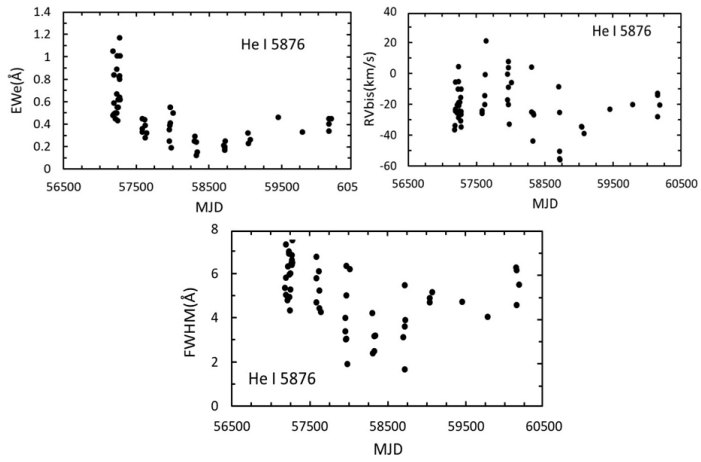

Fig. 5. Time variability in parameters EW_e, RV_{bis} and FWHM for the HeI 5876 line.

rapid variability over several hours, or even days. A similar characteristic time of variability is also observed in the $H\beta$ line profiles. The shortest time of variations is observed between the $H\beta$ line profiles obtained on July 26, 2018 and July 28, 2018, about 2 days.

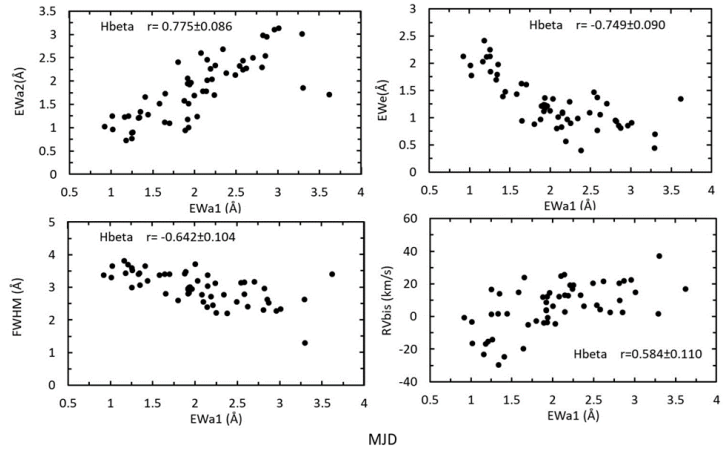

Fig. 6. The spectrophotometric parameters of the Hβ line versus of blue absorption equivalent widths EW_{a1}. The values of the correlation coefficient r and its error for each relations are given on the panels.

6. PHδTOMETRICAL VARIABILITY

The published long time series of photometric data of the star HD 190073 are very small. [38] giving 24 nightly average photoelectric brightness estimates relative to the standard star HD 189851 obtained in JD 2439291-2439399 (108 days). The author showed that the star's brightness is variable, and if it is periodic, then the period should be more than 100 days.

Another work on star photometry was published in [10]. The star was observed in the interval JD 2443259-2443389 (130 days), provided 20 nights of observations. Since these works were carried out in different years and different standard stars were used, the magnitudes are given in relative values, it is impossible to combine these data into one series with the previous data of [38] to find the period. Therefore, we used each array separately for this purpose. To search for the period, the program Period 04 [20] was used, which applied Fourier analysis using the method of [30].

In Figure 8 shows, the power spectrum obtained from data [38]. As can be see, only three significant peaks stand out, with frequencies $v_1 = 0.34341/d$ $v_2 = 0.26911$/d and $v_3 = 0.01021$/d, which corresponds to the periods $P_1 = 2.9388$ days, $P_2 = 3.716$ days and $P_3 = 97.9432$ days, respectively.

Period P_2 is less powerful than the other two peaks, and perhaps is the last of the probable periods that can be real. To clarify which of these periods is more realistic, we also used spectral data for analysis.

To analyze periodic changes in the spectrum of the star, we used different values of spectrophotometric parameters, such as the equivalent widths of the absorption and emission components, half-widths, residual intensities, and radial velocities of the emission and absorption components of the Hα and Hβ lines. Figure 9 shows an example of the power spectrum for Hβ lines for different parameters. Almost for most parameters in the power spectrum, we found a frequency $v_2 = 0.2462 \pm 0.0021$/d, which is close to the frequency we discovered from photometric data. In addition, the frequency $v_4 = 0.25781$/d is also observed in a weaker form, which is repeated in most arrays. These frequencies are shown in Fig. 9 by vertical lines. The periods at these frequencies are respectively equal to $P_2 = 4.061 \pm 0.036$ d, $P_4 = 3.8789 \pm 0.767$ d. The frequency v_3 observed from photometric data (Fig. 8) in different spectral parameters is detected in close but divergent frequencies, corresponding to periods of 92-105 days.

In addition, according to the parameters EW_a and EW_e, the strongest peak $v_5 = 0.0108 \pm 0.0002$ is revealed in frequency, which corresponds to the period $P_5 = 92.1 \pm 0.1$ days. Figure 10 shows the phase curves collapsed over this period. As can be seen, for individual parameters there is a satisfactory picture of periodicity.

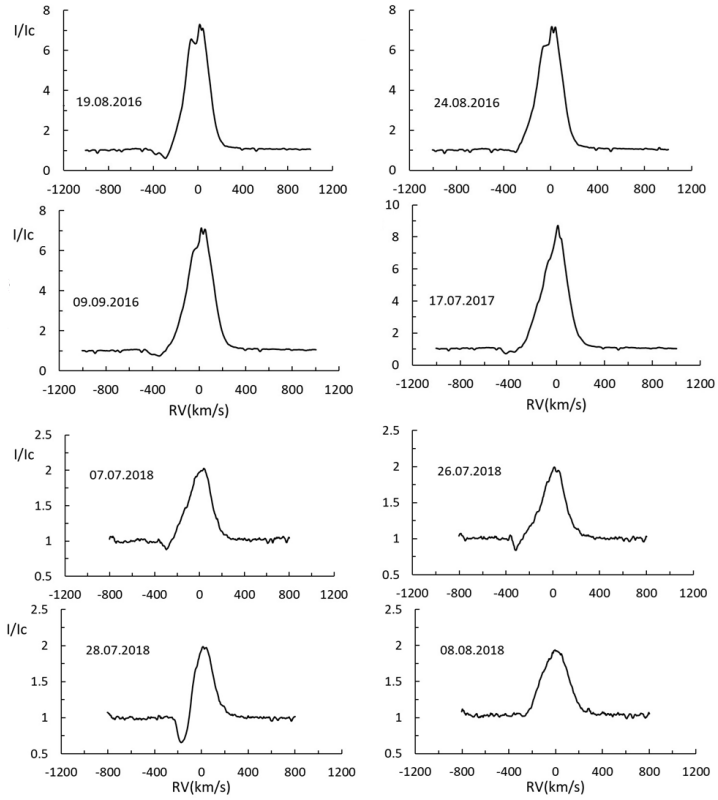

Fig. 7. Hα (above) and Hβ (below) line profiles, presented for different dates, extracted from photospheric radiation.

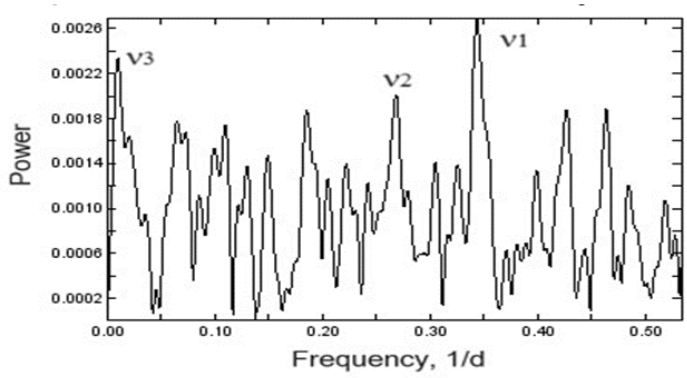

Fig. 8. Power spectrum according to photometric data [38].

Thus, statistical Fourier analysis carried out on photometric and spectral data showed that it is possible that there are several periodic components, which to-

gether give an overall complex picture of the variability of both the spectrum and the brightness of the star. The most probable periods are $P_2 = 4.06 \pm 0.2$ days and $P_5 = 92.1 \pm 0.5$ days.

7. SPECTRAL ENERGY DISTRIBUTION

For analysis of the spectral energy distribution (SED) of the star, we constructed a SED curve of the star in the wavelength interval 0.36-100 μm. The starting material for constructing the SED curves was multicolor broadband photometry data in the standard UBVRIJHKLM system; for the region of longer waves we used data from the WISE W1-W4 infrared (IR) satellite [17], as well as IRAS data [24], respectively, in the bands of 12, 25, 60, 100 μm. The principle of constructing SED for different objects based on stellar magnitudes obtained in different bands of broadband photometry is to convert the magnitudes m_λ into absolute fluxes F_λ according to the famous expression

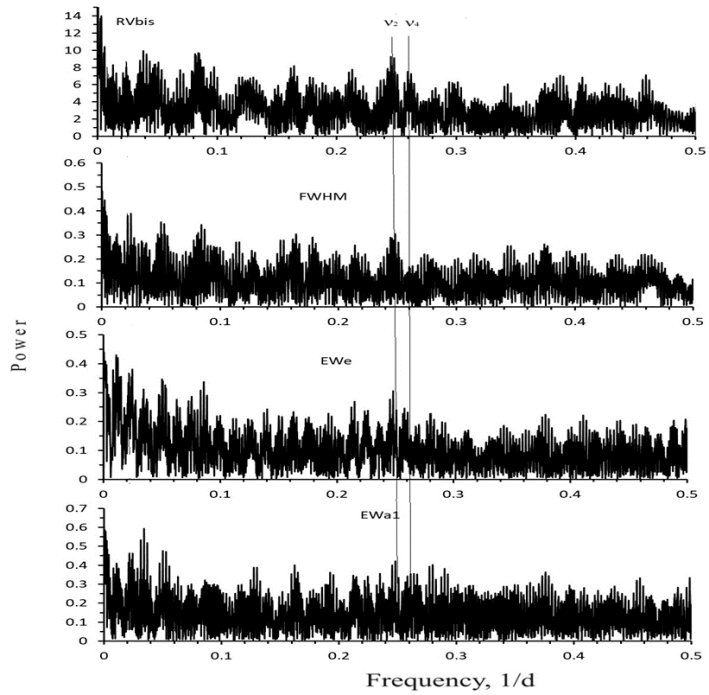

Fig. 9. Examples of power spectrum diagrams for different spectral parameters of the H_β line. Vertical lines show the positions of frequencies ν_2 and ν_4.

$$F_\lambda = F_0 \cdot 10^{-0.4(m_\lambda - m_0)} \quad (1)$$

Here F_0 is the adapted radiation flux for the zero point of the system when m_0 is taken equal to zero. The reference is usually made to the adapted absolute radiative flux of a standard star of zero magnitude A0V in all emission bands. We described the detailed methodology for constructing the SED curve in the work of Ismailov et al. [15, 16].

As can be seen from Fig.11 , the SED curve agrees well with observations only in the visible and near IR region up to the K band (2.2μ m). Excess emission from the gas component of the disk mainly begins from this band.

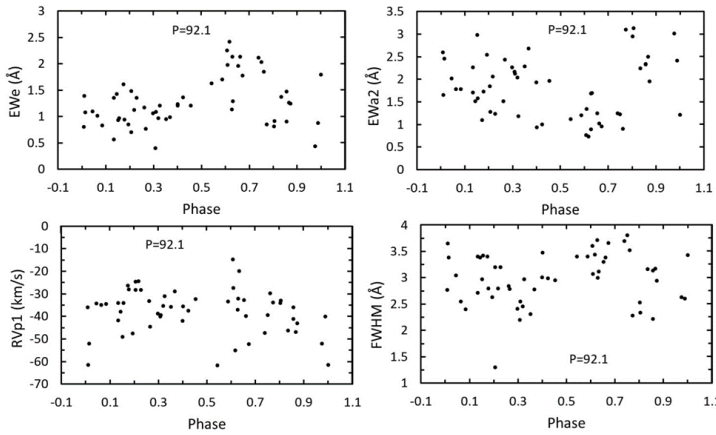

Fig. 10. Examples of phase curves collapsed by phases of the period $P_5 = 92.1$ days.

We have collected in Table 1 some physical parameters of the star, including the values we determined for $T_{\rm eff}$ and log g. Using the magnitude V cleared of interstellar reddening, the distance to the star, and the bolometric correction taken from [26], the absolute bolometric magnitude M_{vb} was calculated (Table 1). Knowing the solar absolute luminosity $M_{vb\odot} = 4.83\,mag$, we calculated the absolute luminosity of the star in units of $L/L_{\odot}$. Next, knowing the effective temperature and luminosity, we calculated the radius of the star $\mathrm{R} = 10.4 \pm 0.6\mathrm{R}\odot$. The solar effective temperature $T_{eff\odot}$ was taken equal to 5800 K .

Using theoretical evolutionary tracks [6, 21] the mass and age of the star were also determined. Figure 12 shows the evolutionary diagram of HR where the position of the star HD 190073 is marked with a circle. The mass and age determined from this diagram are given in Table 1.

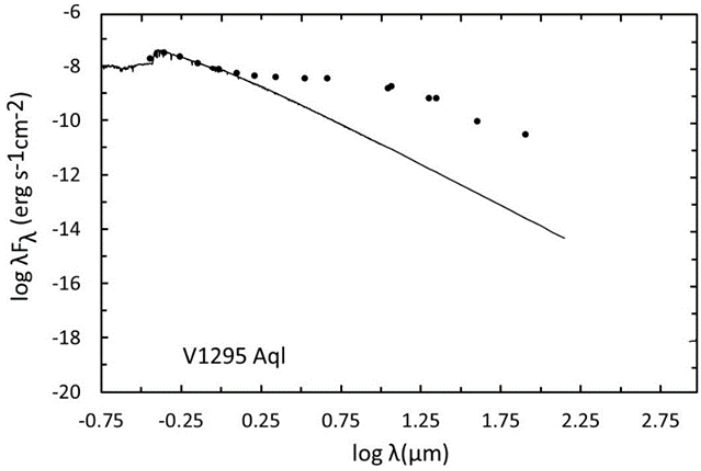

Fig. 11. . Spectral energy distribution for HD190073. Solid curve-Kurucz model with T_{eff} = 9000 K , log g =3.0. Points are observational data.

Table 1. Main physical parameters of the HD 190073.

T_{eff}	log g	V	Av	D,pc	Mb	Mvb	Log $L/L_\odot$	$M/M_\odot$	t,Myr
9000	3.0	7.73	0.40	847	-0.15	-2.16	2.79	4.2	0.9
±250	±0.3		+0.12	±22		±0.15	±0.12	±0.25	±0.2
			-0.26						
		[22]	[39]	[11]	[26]				

8. DISCUSSION AND CONCLUSIONS

Summarizing the results obtained in the 2 nd article, in conclusion we will highlight the most important conclusions of this work. Complementing the studied spectral material with a resolution of 28000, which were obtained for 2016-2023. We managed to find the answer to some questions observed in the spectrum of the star.

By using the Balmer line profiles we were able to select a synthetic spectrum corresponding to the effective temperature and gravitational acceleration $T_{\rm eff} = 9000 \pm 250$ K, $\log g = 3.0 \pm 0.1$, at [Fe/H] = 1.0. After selecting such a model, we determined the extracted profile (star minus standard) in the H and K CaII lines. We have shown that the extracted profile of ionized calcium lines has a typical of the P Cyg type profile, and in general does not differ much from the profiles of hydrogen lines. The structure of these lines showed that there is a strong outflow of matter with a velocity of over 300 km/s. Analysis of the difference profiles of hydrogen lines showed that a dense mass of matter ejected

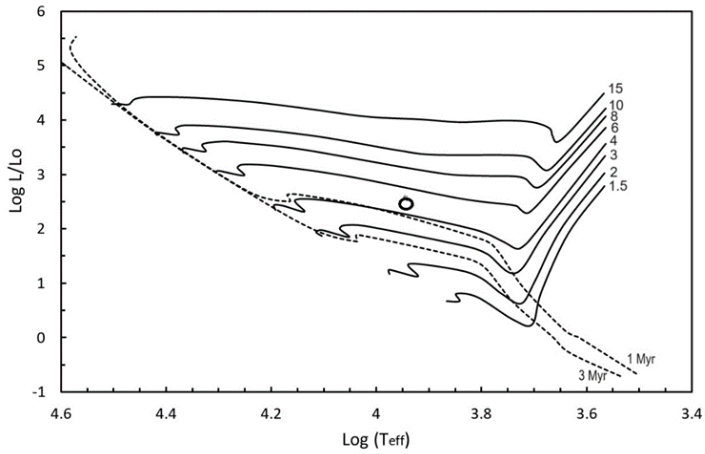

Fig. 12. Position of the star on the HR diagram, with evolutionary tracks, constructed in the works of . [6, 12] Solid lines indicate masses, dotted lines indicate ages.

and directed along the magnetic field lines forms a deep absorption component. Over time, the ejected mass at high latitudes becomes rarefied and accretes to the surface of the star, forming weak emission components on the blue wing of the profile. These components are unstable and gradually merge with the main emission, which is formed from the radiation of the disk. We were able to determine the intensity ratio of the hydrogen lines $H\alpha : H\beta : H\gamma : H\delta$ as 6.17:1.04:0.65:0.42. This shows that the Balmer decrement is too steep, apparently caused by valuable interstellar and/or circumstellar reddening.

Long-term variability of spectrophotometric parameters is detected for the lines of hydrogen, helium and other elements. On the character of the long-term variability over time, there is a general cycle of about 38-12 years. A stellar companion or massive planets may cause the reasons for such variations.

A correlation was found in certain parameters with the intensity of the blue absorption component. This indicates that the main mechanism of activity is the accretion process.

We were able to conduct a Fourier analysis of the star's brightness and spectrum. Based on the variations in brightness, three most probable periods of variability have detected. Analysis of the Fourier spectrum showed a complex nature of variability. Some periods found in the spectrum and brightness are close and determined with high reliability. From short periods $P_2 = 4 \pm 0.5$ days, and from relatively long periods $P_3 = 97 \pm 3$ days are reliably established.

We plotted a star SED curve in the wavelength range $0.36 - 100\mu$ m. It is shown that there is excess radiation characteristic of cold dust in the far IR part of the spectrum. In addition, an excess of radiation in the spectrum is also observed

in the near-IR part of the spectrum, which is characteristic of gas radiation. Using updated literature data and our results, all the fundamental parameters of the star and its evolutionary status were determined.

REFERENCES

1. Aarnio A.N., Monnier J.D., Harries T.J. et al. 2017, ApJ **848**, 18.
2. Acke B., Waelkens C. 2004, A&A, **427**, 1009.
3. Alecian E., Neiner C., Mathis S., Catala C., Kochukhov O., Landstreet, J. 2013, A&A, **549**, L8.
4. Bashirova U.Z., Adigozalzade H.A., Ismailov N.Z.. 2024, AAJ, **19**, 15.
5. Bouvier J., Alencar S.H.P., Harries T.J., Johns- Krull C.M., Romanova M.M., in Protostars and Planets V, eds. B. Reipurth, D. Jewitt & K. Kaul (Tucson: Univ. Arizona Press), 2007, **479**, 328.
6. Bressan A., Marigo P., Girardi L. et al. 2012, MNRAS, **427**, 127.
7. Catala C., Alecian E., Donati J.-F. et al. 2007, A&A, **462**, 293.
8. Cowley C.R., Hubrig S., 2038, Bull.' of the AAS, **43**, 102.
9. Cowley C.R., Hubrig S. 2012, AN **333**, 34.
10. Deul E.R., van Genderen A.M., 1983, A&A, **388**, 289.
11. Gaia collaboration 2020 yCat, 1350, 0G.
12. Gullbring E., Hartmann L., Brice no C., Calvet N. 1998, ApJ , **492**, 323.
13. Hubrig S., Carroll T.A., Schöller M., Ilyin I. 2015, MNRAS, **449**, L388.
14. Hubrig S., Schöller M., Ilyin I., Lo Curto G. 2013, Astron. Nachr., **334**, 1093.
15. Ismailov N.Z., Valiyev U.S. 2022, Astron. Repor., **66**, 965.
16. 16.Ismailov N.Z/, Kholtygin A.F., Romanyuk I.I., Pogodin M.A. 2021, AAJ, **16**, 5.
17. Jarrett T.H., Cohen M., Masci F., et al., 2038, Astrophys . J., **382**, 735.
18. Königl A. 1991, ApJ ,**370**, L39.
19. Kozlova O.V., Pogodin M.A., Alekseev I.Yu. , et al., 2019, Astrophys., **62**, 38.
20. Lenz P., Breger M. 2005, CoAst, **146**, 53.

21. Marigo P., Girardi L., Bressan A., et al. 2017, ApJ , **835**, 77.

22. Mendigutia I., Mora A., Montesinos B., et al., 2012 A&A, **543**A, 59M.

23. Merrill, P.W. 1933, ApJ , **77**, 51.

24. Neugebauer G., Habing H. J., van Duinen R., et al., 1984, Ap J. **278**, L1.

25. Paatz G., & Camenzind M. 1996, A&A, **308**, 77.

26. Pecaut M.J. and. Mamajek E. E. 2013, AJSS, **208**, 22.

27. Pogodin M., Franco G.A.P., Lopes D.F., 2005 A& A, **438**, 239.

28. Pogodin M.A, Drake N.A., Beskrovnaya N.G., et al., 2021, Universe, **7**, 489.

29. Scargle J.D. 1973, ApJ , **179**, 705.

30. Scargle J.D. 1982, ApJ , **263**, 835.

31. Straizys V., Kuriliene G. 1981, Ap&SS, **80**, 353.

32. Struve O., & Swings P. 1942, ApJ , **96**, 475.

33. Surdej J., & Swings J.P. 1976a, A&A, **47**, 383.

34. 34.Surdej J., & Swings J.P. 1976b, A&A, **47**, 121.

35. Surdej J., & Swings J.P. 1977, A&A, **54**, 219.

36. Swings P., & Struve O. 1940, ApJ , **91**, 546.

37. Tifft W. G. 1977, ApJ , **238**, 377.

38. Van Genderen AM 1971, A&A **14**, 48.

39. Vioque M., Oudmaijer R.D., Baines D. et al. 2018, A&A, **620**, 17.

40. Wichittanakom C., Oudmaijer R.D., Fairlamb J.R., et al., 2020, MNRAS **493**, 234.